Progress In Electromagnetics Research B, Vol. 26, 451–469, 2010

COUPLED LINES FROM FILTER TO COMPOSITE RIGHT/LEFT HANDED-CELLS

A. M. E. Safwat

Faculty of Engineering
Electronics and Communication Engineering Department
Ain Shams University, Cairo, Egypt

T. M. Abuelfadl

Faculty of Engineering
Electronics and Electrical Communication Engineering Department
Cairo University, Giza, Egypt

Abstract—This paper studies the left-handed behavior in conventional 2-port coupled line networks. The propagation parameters of 12 periodic structures, each has a different coupled line configuration, have been derived and the left-handed bands have been determined. Two structures were fabricated and measured to confirm the composite right/left handed (CRLH) characteristics. Measurements and EM simulations were in a very good agreement with the developed theory. In the light of the proposed theory, a geometrical circuit model was also proposed for split ring resonator (SRR). The model is capable to predict its performance over a wide band.

1. INTRODUCTION

CRLH structures is a new category of microwave passive devices that allows the implementation of transmission lines that have left-handed (LH) bands, where the phase and group velocities have opposite directions. Current implementations of CRLH structures include, but not limited to, lumped components, commercial-off-the-shelf components, split-ring resonators and tunable devices [1–3].

Along the past few decades, coupled lines have been extensively studied. Interestingly, not all their features have been yet explored [4–6]. From filter theory to composite right/left handed (CRLH)

Received 28 September 2010, Accepted 29 October 2010, Scheduled 16 November 2010
Corresponding author: Amr M. E. Safwat (asafwat@ieee.org).

structures, coupled lines have been considered as valuable microwave components [7–10].

Recently the authors had proposed separately the use of different 2-port coupled line networks as CRLH unit cells [8, 10]. This paper extends that work to cover the twelve different configurations of the 2-port coupled line networks and presents, within the light of the coupled line theory, a simplified model for split ring resonators (SRR).

2. THEORY

2.1. Analysis of Periodic Structures

Periodic structures, examples are shown in Fig. 1, are characterized by two parameters: the propagation constant, β, and the Bloch impedance, Z_B, which reduces to the characteristic impedance when the homogeneity condition applies:

$$p \ll \lambda, \tag{1}$$

where p is the pitch size and λ is the wavelength. Both parameters are extracted from the ABCD parameters of the constituent unit cell as follows [11]:

$$\beta = \frac{1}{p}\cos^{-1}\frac{A+D}{2} \tag{2}$$

$$Z_B^{\pm} = \frac{2B}{(A-D) \mp \sqrt{(A-D)^2 - 4}} \tag{3}$$

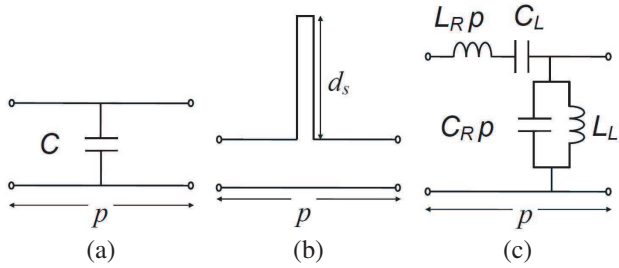

Figure 1. Unit cell of (a) capacitively loaded TL, (b) TL periodically loaded with series stubs (d_s is the length of the stub), (c) CRLH TL (C_L and L_L are the left handed capacitance and inductance respectively and C_R and L_R are the per unit length right-handed capacitance and inductance respectively, p is the pitch.

2.2. Dispersion Relation of Conventional Periodic Structures

Figure 2 shows the dispersion relation of the conventional capacitively loaded transmission line depicted in Fig. 1(a). It is assumed that the propagation velocity in the host transmission line is the speed of light in free space, c, and that the capacitors are lumped. The first Brillouin zone is defined by the boundaries, $-\pi \leq \beta p \leq \pi$. Below the Bragg frequency, f_B, defined as $\frac{2\pi f_B p}{c} = \pi$, the fundamental component of the incident wave (v_g is +ve), a_0, is right handed (RH) (shown in yellow). The spatial harmonic (a_1) is RH, (shown in yellow), and the spatial harmonic (a_−1) is LH, (shown in gray). Higher harmonics have the same pattern. The same is for the reflected wave, the fundamental component of the reflected wave (v_g is −ve) is RH (shown in green). The spatial harmonics alternate between RH and LH.

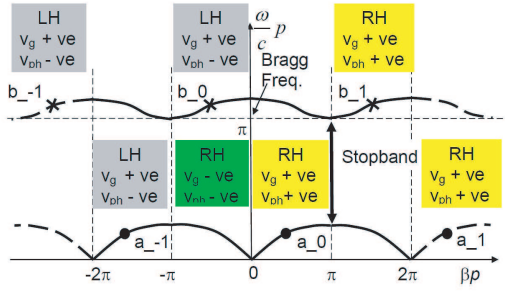

Figure 2. Dispersion relation of a capacitively loaded transmission line. (v_g and v_{ph} are the group and phase velocities, respectively. +ve and −ve stand for postive and negative values.).

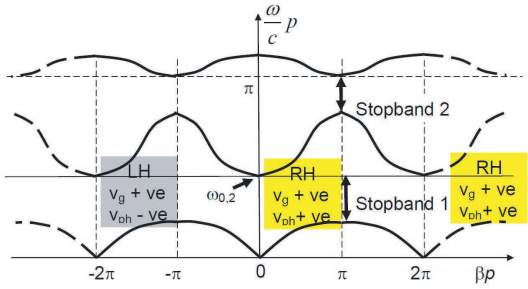

Figure 3. Dispersion relation of a transmission line periodically loaded with series stubs. The length of the stub, d_s, is longer than the pitch.

Above f_B, the fundamental component of the incident wave (v_g is +ve), b_0, is LH (shown in gray). The spatial harmonic (b_1) is RH, (shown in yellow), and the spatial harmonic (b_−1) is LH (shown in gray). Higher harmonics have the same pattern. A stopband appears between the first RH band and the first LH band.

If the transmission line is periodically loaded with series short-circuited stubs, Fig. 1(b), a number of RH bands will appear before f_B as long as the length of the stubs is longer than the pitch [11]. Fig. 3 shows the dispersion relation in this case. At $\omega_{0,2}$, the length of the stub is $\lambda/2$.

2.3. Dispersion Relation of CRLH Structures

Pure LH transmission line should have a LH band that extends over the entire frequency band. Unfortunately, such line does not exist. In practice, capacitors and inductors are inserted in a host transmission line, as shown in Fig. 1(c), to create the LH band. Fig. 4 shows the dispersion relation of CRLH transmission lines. Unlike the conventional periodic structures, the LH band appears below f_B, i.e., the fundamental component of the incident wave b_0 is LH (shown in gray). The CRLH unit cell is said to be balanced when a smooth transition between the LH band and the RH band (a_0) is achieved.

Beside the lumped elements implementation, other approaches have been adopted in the literature to create LH bands below f_B. In the dual CRLH [1], the first band was RH while the second was LH. Balance condition could not be achieved. A generalized resonance circuit was proposed in [2] to create a generalized negative refractive index transmission line. Varactors were used in [12] to

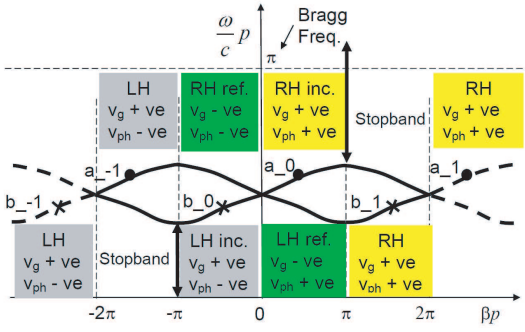

Figure 4. Dispersion relation of a CRLH transmission line. The fundamental (b_0) and the first harmonic (b_−1) of the incident (inc.) wave are LH, while the first harmonic (b_1) is RH. The same is applied for the reflected (ref.) wave.

implement tunable CRLH transmission lines. In [13], long open-circuited parallel stubs and short circuited series stubs were inserted in the host transmission line to create LH bands in the stopbands shown in Fig. 3. The resulting operation bands alternate between dual and conventional CRLH Transmission lines. From the point of view of left-handed operation, these stubs can be considered as complement, the series stubs create negative permittivity frequency bands while the shunt stubs create negative permeability frequency bands. Similar performance was obtained in [8].

3. COUPLED LINE UNIT-CELLS

In the classical paper of Jones and Bolljahn, published in 1956 [4], 10 coupled-line networks were studied for filter and coupler applications. For each configuration, they derived the image impedance and determined the operating bands assuming that the velocities of the even and odd modes are equal, i.e., homogeneous medium. In [5], Zysman and Johnson studied the same structures when the medium is inhomogeneous. In this paper, we have:

(i) added two more structures (diagonal connected, same line connected) to complete the 2-port coupled line networks,

(ii) studied the dispersion relation of each network,

(iii) determined the LH bands that appear below f_B,

(iv) proposed CRLH transmission lines using the 2-port coupled lines networks, and

(v) explained the operation of the split ring resonators in the light of the proposed theory.

Table 1. Same side connections, the propagation constants are plotted in black solid line, while Bloch impedance are in gray dotted line.

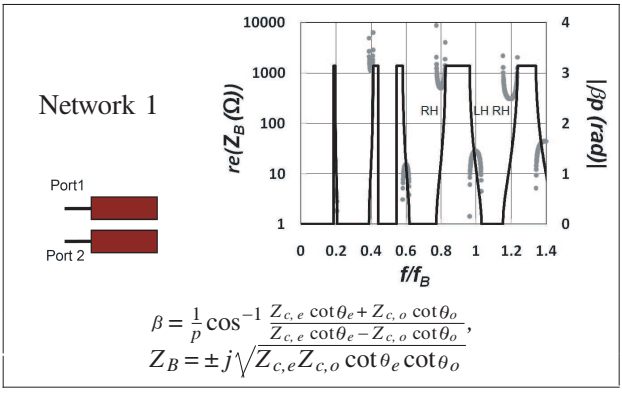

$$\beta = \frac{1}{p}\cos^{-1}\frac{Z_{c,e}\cot\theta_e + Z_{c,o}\cot\theta_o}{Z_{c,e}\cot\theta_e - Z_{c,o}\cot\theta_o},$$
$$Z_B = \pm j\sqrt{Z_{c,e}Z_{c,o}}\cot\theta_e\cot\theta_O$$

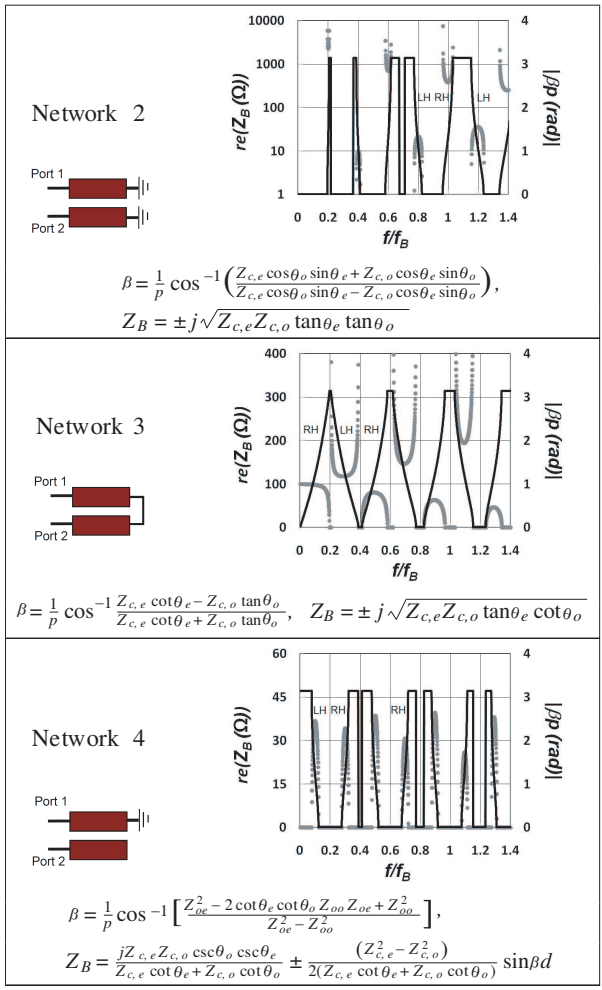

In this paper, the 2-port coupled line networks have been divided into three categories: same side, diagonal and same line connections, depending on the relative positions of the input/output ports. The other two ports have one of the following connections: open-open, short-short, short-open, or connected together. These result in 12 networks. Schematics are shown in Tables 1, 2, and 3. The same side cases are shown in Table 1, the diagonal cases are shown in Table 2, and the same line cases are shown in Table 3. Compact configurations for network 5 and network 9 are shown in Tables 2 and 3, respectively.

The propagation constants were derived according to Eq. (2) and they are plotted in black solid line, while, the Bloch impedances were derived according to Eq. (3) and they are plotted in gray dotted line.

Circuit simulations were carried out using ANSOFT designer student version. Physical microstrip coupled lines were considered to include the difference between the propagation velocities of the even and odd modes. The separation between the coupled lines, S, and the width, W, are 0.5 mm and 1 mm, respectively. The length of the coupled lines, l, is 40 mm, and the substrate is RT/Duroid 5870 (the substrate height, h, is 1.6 mm and the relative dielectric constant, ϵ_r, is 2.33). These dimensions correspond to $Z_{c,e} = 148\,\Omega$, $Z_{c,o} = 71\,\Omega$, $\epsilon_{e,e} = 1.897$, and $\epsilon_{e,o} = 1.686$ at 2 GHz, where $Z_{c,e}$ and $Z_{c,o}$ are the characteristic impedances and $\epsilon_{e,e}$ and $\epsilon_{e,o}$ are the effective dielectric constants of the even and odd modes respectively. The pitch size, p, defined as the separation between two consecutive coupled lines in the longitudinal direction, was chosen to be 15 mm to ensure that the LH bands appear

Table 2. Diagonal connections, the propagation constants are plotted in black solid line, while Bloch impedance are in gray dotted line.

Network 5

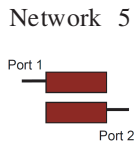

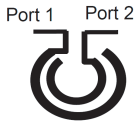

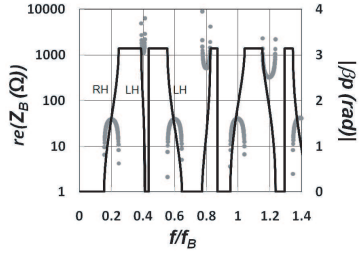

$$\beta = \frac{1}{p}\cos^{-1}\left(\frac{Z_{c,e}\cot\theta_e + Z_{c,o}\cot\theta_o}{Z_{c,e}\csc\theta_e - Z_{c,o}\csc\theta_o}\right),$$

$$Z_B = \pm\frac{1}{2}\sqrt{Z_{c,e}^2 + Z_{c,o}^2 - \frac{2Z_{c,e}Z_{c,o}(1+\cos\theta_e\cos\theta_o)}{\sin\theta_e\sin\theta_o}}$$

Network 6

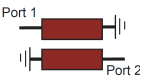

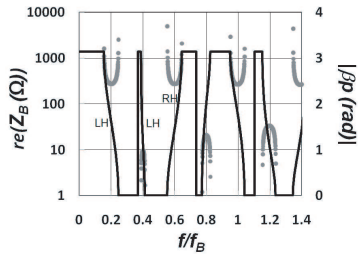

$$\beta = \frac{1}{p}\cos^{-1}\left(\frac{Z_{c,e}\sin\theta_e\cos\theta_0 + Z_{c,o}\sin\theta_o\cos\theta_e}{Z_{c,e}\sin\theta_e - Z_{c,o}\sin\theta_o}\right),$$

$$Z_B = \frac{\pm 2Z_{c,e}Z_{c,o}}{\sqrt{Z_{c,e}^2 + Z_{c,o}^2 - \frac{2Z_{c,e}Z_{c,o}(1+\cos\theta_e\cos\theta_o)}{\sin\theta_e\sin\theta_o}}}$$

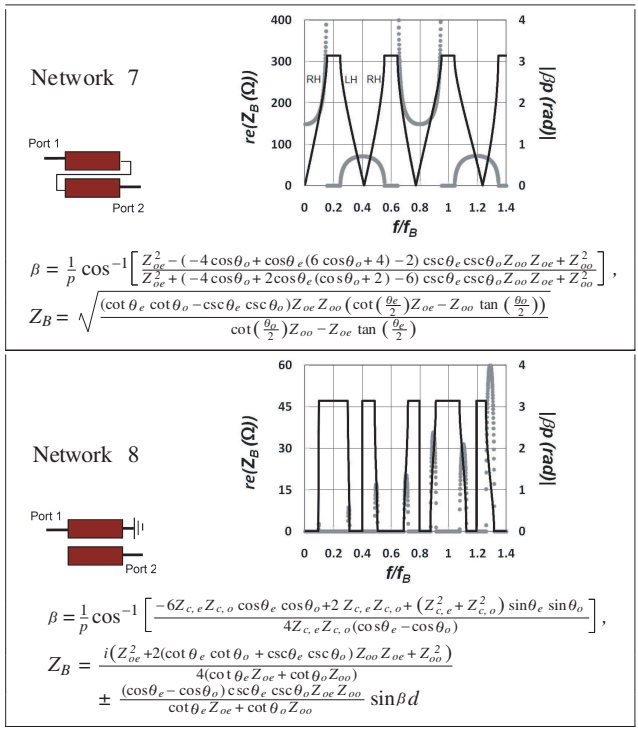

$$\beta = \frac{1}{p}\cos^{-1}\left[\frac{Z_{oe}^2 - (-4\cos\theta_o + \cos\theta_e(6\cos\theta_o + 4) - 2)\csc\theta_e \csc\theta_o Z_{oo} Z_{oe} + Z_{oo}^2}{Z_{oe}^2 + (-4\cos\theta_o + 2\cos\theta_e(\cos\theta_o + 2) - 6)\csc\theta_e \csc\theta_o Z_{oo} Z_{oe} + Z_{oo}^2}\right],$$

$$Z_B = \sqrt{\frac{(\cot\theta_e \cot\theta_o - \csc\theta_e \csc\theta_o) Z_{oe} Z_{oo} \left(\cot\left(\frac{\theta_e}{2}\right) Z_{oe} - Z_{oo} \tan\left(\frac{\theta_o}{2}\right)\right)}{\cot\left(\frac{\theta_o}{2}\right) Z_{oo} - Z_{oe} \tan\left(\frac{\theta_e}{2}\right)}}$$

$$\beta = \frac{1}{p}\cos^{-1}\left[\frac{-6Z_{c,e}Z_{c,o}\cos\theta_e \cos\theta_o + 2Z_{c,e}Z_{c,o} + \left(Z_{c,e}^2 + Z_{c,o}^2\right)\sin\theta_e \sin\theta_o}{4Z_{c,e}Z_{c,o}(\cos\theta_e - \cos\theta_o)}\right],$$

$$Z_B = \frac{i\left(Z_{oe}^2 + 2(\cot\theta_e \cot\theta_o + \csc\theta_e \csc\theta_o) Z_{oo} Z_{oe} + Z_{oo}^2\right)}{4(\cot\theta_e Z_{oe} + \cot\theta_o Z_{oo})} \pm \frac{(\cos\theta_e - \cos\theta_o)\csc\theta_e \csc\theta_o Z_{oe} Z_{oo}}{\cot\theta_e Z_{oe} + \cot\theta_o Z_{oo}} \sin\beta d$$

Table 3. Same line connections, the propagation constants are plotted in black solid line, while Bloch impedance are in gray dotted line.

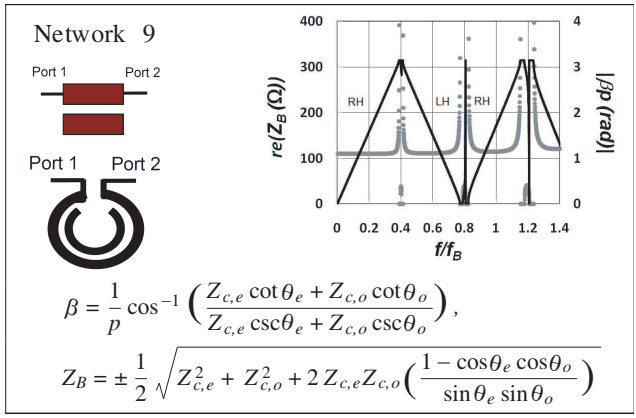

$$\beta = \frac{1}{p}\cos^{-1}\left(\frac{Z_{c,e}\cot\theta_e + Z_{c,o}\cot\theta_o}{Z_{c,e}\csc\theta_e + Z_{c,o}\csc\theta_o}\right),$$

$$Z_B = \pm\frac{1}{2}\sqrt{Z_{c,e}^2 + Z_{c,o}^2 + 2Z_{c,e}Z_{c,o}\left(\frac{1 - \cos\theta_e \cos\theta_o}{\sin\theta_e \sin\theta_o}\right)}$$

Network 10

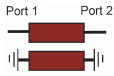

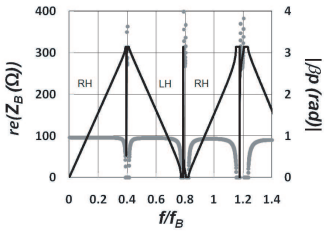

$$\beta = \frac{1}{p}\cos^{-1}\left(\frac{Z_{c,e}\cot\theta_o + Z_{c,o}\cot\theta_e}{Z_{c,e}\csc\theta_o + Z_{c,o}\csc\theta_e}\right),$$

$$Z_B = \frac{\pm 2Z_{c,e}Z_{c,o}}{\sqrt{Z_{c,e}^2 + Z_{c,o}^2 + 2\,Z_{c,e}Z_{c,o}\left(\dfrac{1-\cos\theta_e\cos\theta_o}{\sin\theta_e\sin\theta_o}\right)}}$$

Network 11

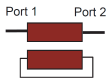

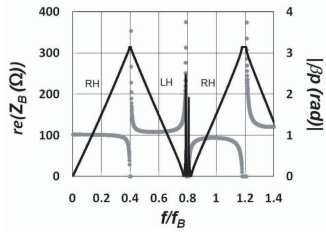

$$\beta = \frac{1}{p}\cos^{-1}\left[\frac{4Z_{c,e}Z_{c,o}(\csc\theta_e\csc\theta_o - \cot\theta_e\cot\theta_o)}{2(Z_{c,e}Z_{c,o}\csc\theta_e\csc\theta_o(\cos\theta_e(4-6\cos\theta_o)+4\cos\theta_o-2)+Z_{oe}^2+Z_{oo}^2)}\right.,$$

$$\left. + \frac{Z_{c,e}^2(3\cos\theta_e - 1)\sec^2\left(\frac{\theta_e}{2}\right) + Z_{c,o}^2(3\cos\theta_o - 1)\sec^2\left(\frac{\theta_o}{2}\right)}{2(Z_{c,e}Z_{c,o}\csc\theta_e\csc\theta_o(\cos\theta_e(4-6\cos\theta_o)+4\cos\theta_o-2)+Z_{oe}^2+Z_{oo}^2)}\right]$$

$$Z_B = \frac{(Z_{oe}Z_{oo}\csc(\theta_e)\csc(\theta_o)(\cos(\theta_e)(4-6\cos(\theta_o))+4\cos(\theta_o)-2)+Z_{oe}^2+Z_{oo}^2)}{4\left(Z_{oe}\tan\left(\frac{\theta_e}{2}\right)+Z_{oo}\tan\left(\frac{\theta_o}{2}\right)\right)}$$

Network 12

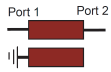

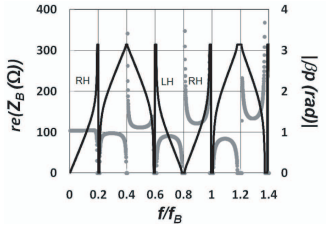

$$\beta = \frac{1}{p}\cos^{-1}\left[\frac{6\cos\theta_e\cos\theta_o Z_{oe}Z_{oo} + 2\,Z_{oe}Z_{oo} - \sin\theta_e\sin\theta_o(Z_{oe}^2+Z_{oo}^2)}{4(\cos\theta_e+\cos\theta_o)Z_{oe}Z_{oo}}\right],$$

$$Z_B^{\pm} = -\frac{i(Z_{oe}^2+2(\cot\theta_e\cot\theta_o-\csc\theta_e\csc\theta_o)Z_{oo}Z_{oe}+Z_{oo}^2)}{4(\cot\theta_eZ_{oe}+\cot\theta_oZ_{oo})}$$
$$\pm\frac{(\cos\theta_e+\cos\theta_o)\csc\theta_e\csc\theta_oZ_{oe}Z_{oo}}{\cot\theta_eZ_{oe}+\cot\theta_oZ_{oo}}\sin\beta d$$

before f_B. The host medium is a microstrip transmission line. For RT/Duroid 5870, the effective dielectric constant, ϵ_e, is 1.98 at 2 GHz and f_B is 7 GHz. In the dispersion relations, depicted in Tables 1–3, the frequency is normalized to f_B.

Frequencies, which correspond to $\lambda/4$ and its multiples are critical in the analysis. Along the paper, they are called transition frequencies. For the even mode, these frequencies normalized to f_B occur at $f_{e,i} = 0.1945, 0.349, 0.5835, \ldots$ where $i = 1, 2, 3, \ldots$ while for the odd mode they occur at $f_{o,i} = 0.2063, 0.4126, 0.6189, \ldots$ where $i = 1, 2, 3, \ldots$. The three coupled line categories are studied from three different perspectives: filter, CRLH, and realization.

3.1. Same Side Connection

Filter behavior: For homogeneous medium, networks 1 and 2 are all-stop filters, network 3 is an all-pass filter, and network 4 is a bandpass filter [4]. If the medium is inhomogeneous, as in this paper, the difference between the propagation velocities of the even and odd modes creates very narrow bands below f_B in networks 1 and 2.

CRLH behavior: For the open-open connection (network 1), the bands below f_B are consecutively LH, RH, LH and RH, while in the short-short connection (network 2), they are RH, LH, RH and LH. In network 3, where the two terminals are connected together, the operating bands are wide and they alternate between RH and LH. As was explained in [8], the odd and even modes of the coupled lines see short and open-circuited stubs respectively. When the length of the coupled line is longer than $\lambda/4$, the equivalent circuit model of the coupled lines stubs is identical to Fig. 1(c), and consequently a LH band appears. After, $\lambda/2$, the coupled lines retain their impedances at low frequencies and the RH band appears. Network 4 is an asymmetrical one. It can be seen as if it has two stubs, one is short-circuited and the other is open-circuited, and they are coupled distributively [10, 14]. At the first transition frequency, the equivalent circuit is close to Fig. 1 and a LH band appears. The bandwidth is larger than networks 1 and 2 since it does not depend on the difference between the velocities of the two modes. At the second transition frequency, a RH band appears. Similar to previous networks, this performance is repeated twice before f_B.

Realization: Networks 1 and 2 passbands solely depend on the difference between the even and odd electrical lengths. Moreover, the rate of change of Z_B is very large. Therefore, it is almost impossible to match the unit cell. Matching can be easily achieved in network 3 (meander type) by tuning the unit cell parameters as was shown in [9]. In network 4, it is asymmetric and consequently Z_B is complex. Matching can only be achieved if two mirrored cells are cascaded [10, 14].

3.2. Diagonal Connection

Filter behavior: Networks 5 and 6 are both band-pass filters [4]. The operating bands appear around the transitions frequencies. Network 7 (diagonal connected) is a low-pass filter. Network 8, (short-open connection) is an all-stop filter [4]. However in this case, the difference between the velocities of the even and odd modes creates very narrow bands near the transition frequencies.

CRLH behavior: The first operating band in the open-open connection (network 5) is RH, while the second, which appears around the second transition frequency, is LH and it is very narrow. A second LH band appears around the third transition frequency. A second RH band appears at the fourth transition frequency. The short-short connection (network 6) has different behavior. The first two bands are LH while the third and fourth bands are RH. In network 7, the bands alternate between RH and LH. Stop bands appear at the odd transition frequencies. Unlike networks 5 and 6, wide operating bands and smooth transition between LH and RH bands can be achieved near the even transition frequency, where the stub length is multiple of $\lambda/2$. Network 8 is asymmetric. The operating bands are very narrow, and they alternate between RH and LH.

Realization: Z_B in network 5 and 6 is very dispersive and consequently it is expected that the operating band will be very narrow. Moreover, Z_B in network 6 is pretty high. This will enforce the use of high dielectric constant or stripline technology to realize these unit cells. Network 7 is similar to network 3 in terms of the wide operating bands and the feasible values of the Z_B. Network 8 is asymmetric and consequently Z_B is complex. Similar to network 4, matching can only be achieved if two mirrored cells are cascaded.

3.3. Same Line Connection

Filter behavior: Networks 9–12 are notch filters [4]. The rejected frequencies are multiple of $\lambda/2$ in network 9 and 10, odd multiple of $\lambda/4$ in network 12, and multiple of λ in network 11.

CRLH behavior: In the four networks and similar to network 3, the bands alternate between RH and LH. Unlike network 3, transitions between the bands occur when the length of the coupled lines is multiple of $\lambda/2$. This makes network 3 the best in terms of size.

Realization: The networks in this category have flat operating bands and the value of Z_B is achievable even for the asymmetrical case.

4. EXPERIMENTAL VERIFICATION

Coupled line CRLH transmission lines were fabricated using networks 3 and 4 as unit cells. Network 3 has the smallest size compared to other unit cells that start with RH band. Network 4 is the best in terms of matching compared to other unit cells that start with LH. Measurements were carried out to confirm the theory presented in the previous sections. The design details of network 3 and 4 can be found in [8] and [10] respectively. In this section, their results are summarized.

4.1. Network 3 (Meander Coupled Lines)

Seven unit cells of network 3 were cascaded on RT/Duroid 5870 ($h = 1.6\,\text{mm}$, $\epsilon_r = 2.33$, $\tan\delta = 0.002$, and copper metallization) as shown in Fig. 5(a) to form a CRLH transmission line. The cells are connected symmetrically to the host line to achieve $50\,\Omega$ Z_B. Fig. 5(b) shows the circuit simulations, EM simulations and measurements [15]. Transitions within $-2\,\text{dB}$ insertion loss were achieved at 1.2 GHz, $\omega_{0,1}$, and 2.4 GHz, $\omega_{0,2}$. At higher transition frequencies, S_{21} drops to less than $-10\,\text{dB}$, while S_{11} increases significantly. Good agreement between circuit and EM simulations was achieved up to 4 GHz. After 4 GHz, deviation between EM and circuit simulations increases, the second LH band is narrower than the expected value, and the total loss is larger. Measurement results are in a very good agreement with EM

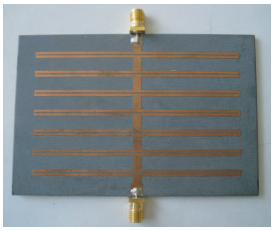

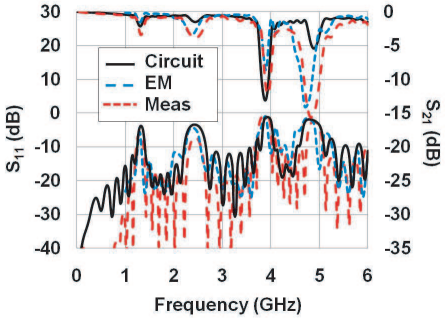

(a) (b)

Figure 5. (a) Picture of the fabricated structure, (b) S-parameters, measurements, circuit and EM simulations, $S = 0.5\,\text{mm}$, $l = 40\,\text{mm}$, $p = 8\,\text{mm}$, $W_m = 3.9\,\text{mm}$ and $W = 1\,\text{mm}$. The substrate is RT/Duroid 5870 ($h = 1.6\,\text{mm}$, $\epsilon_r = 2.33$, $\tan\delta = 0.002$, and copper metallization).

simulations. The difference between the circuit model from one side, and the measurements and EM simulations from the other side, lies in the radiation losses, which cannot be described precisely in circuit simulators.

4.2. Network 4

Network 4 is an asymmetric network, which results in a complex Bloch impedance. Hence matching to a regular RH line with real characteristic impedance is impossible. A symmetrical version of this network can be obtained if the cell is cascaded with its mirrored version as shown in Figs. 6(a) and 6(b). Balanced conditions will be achieved if the difference between the even and odd impedances is sufficiently large, i.e., tight coupled lines. Broadside coupled coplanar waveguide [10] and microstrip coupled lines with ground etching [14] provide this condition.

Figure 7 shows 5 cells CRLH transmission line using broadside coupled coplanar waveguide, where an upper and lower overlays are employed to minimize the difference between the even and odd phase velocities [10]. The substrate is FR4 ($h = 1.6\,\text{mm}$, $\epsilon_r = 4.4$, $\tan\delta = 0.02$, and copper metalization). Fig. 8 shows the EM and circuit simulations. The LH band lies in the frequency range 0.45–0.7 GHz while the RH band is in the range 0.7–1.1 GHz. Experimental results, which are also shown in Fig. 8, agree well with the theoretical expectations. Discrepancy between measurements and simulations is due to the substrate losses.

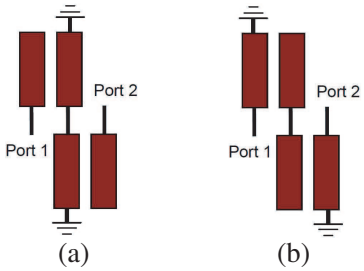

Figure 6. Two configurations of the symmetrical cell formed by cascading the asymmetrical structure network 4 in Table 1, (a) open short open configuration (OSO), (b) short open short configuration (OSO).

(a) top layer (b) bottom layer

Figure 7. CRLH TL with dielectric overlay, composed of 5 cells. The coupled lines are broadside coupled coplanar waveguide.

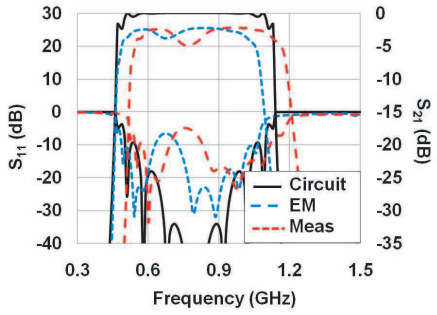

Figure 8. S-parameters, measurements and circuit and EM simulations, of the CRLH TL shown in Fig. 7. $S = 1.6\,\text{mm}$, $l = 47\,\text{mm}$, $p = 27\,\text{mm}$, $W = 1.76\,\text{mm}$, and the gap width between the center strip and the side conductors is 4.77 mm. The substrate is FR4 ($h = 1.6\,\text{mm}$, $\epsilon_r = 4.4$, $\tan\delta = 0.02$, and copper metallization).

5. DISCUSSION

In filters, coupled lines are generally located in the longitudinal direction, and whenever they are connected in the transverse direction, their lengths have never exceeded $\lambda/4$ [16]. Unlike filters, coupled line cells in CRLH transmission lines are located in the transverse direction and their lengths exceed $\lambda/4$ to get the LH properties. Moreover, p has to be smaller than the guided wavelength in the host transmission line. This allows the implementation of microwave components that can not be realized using conventional transmission line, e.g. arbitrary coupling directional coupler as was shown in [9].

Interestingly, split ring resonators, which are conventional metamaterial components, can also be described in terms of the proposed theory of the coupled lines. In this section, two points

are addressed: the duality between the coupled line cells and the description of split ring resonators in the light of the coupled line theory.

5.1. Dual Structures

Duality means that bands switch from RH to LH or vice versa [1]. For example, the first operating band in network 1 is LH, while it is RH in network 2. The difference is due the loads, network 1 has an open-open connection, while network 2 has short-short connection. Unfortunately, the response of networks 1 and 2, depends on the difference between the velocities of the even and odd modes. If they are equal, both networks are all-stop filters.

Networks 5 and 6 have the same duality behavior, i.e., in network 5, the first band is RH while it is LH in network 6. Unlike networks 1 and 2, the response of networks 5 and 6 does not rely on the difference between the velocities of the even and odd modes and the bands are wide. At low frequencies, the ports in both networks are separated by a distributed capacitor. However, in network 5 the ports simultaneously see open-circuited stubs, and therefore the behavior is RH. While in network 6, the ports see short-circuited stubs, and consequently the overall equivalent circuit is similar to Fig. 1(c), and the performance is LH.

5.2. Split Ring Resonators

Split ring resonators (SRRs) behave as magnetic dipoles. When present in a host transmission line, they emulate a medium with negative permeability [17]. SRRs come in different shapes, e.g., edge coupled, non-bianisotropic, and open [18]. These are shown in Figs. 9(a)–9(c) respectively. In fabrication, SRRs are patterned on one metal side of the laminate while the metal beneath them on the other side of the laminate is removed. The equivalent circuit model is a series resonant circuit [19]. To create a LH band, periodic vias are inserted in the host transmission line, and to get balanced CRLH transmission lines, the vias are replaced by complementary SRRs [3].

The proposed coupled line models for the edge coupled, non-bianisotropic, and open-SRRs are shown also in Figs. 9(a)–9(c) respectively. In these models, the metal ground has been removed, i.e., $Z_{c,e}$ tends to a very large value.

The Open (O)SRR, shown in Fig. 9(c), was carefully investigated in [19]. The equivalent inductance and capacitance were 10 nH and 0.24 pF respectively, when the external radius was 2.2 mm, the line width was 0.14 mm, the width of the slot between the two lines was

0.25 mm, and the etched area beneath the OSSR was 9.54 mm × 8 mm. The cell was patterned on an PTFE substrate ($h = 0.49$ mm, $\epsilon_r = 2.43$). This structure can be viewed as identical to network 5 in Table 2. The ABCD matrix of this network can be written as,

$$\begin{bmatrix} A & B \\ C & D \end{bmatrix} = \begin{bmatrix} \frac{Z_{c,e}\cot\theta_e + Z_{c,o}\cot\theta_o}{Z_{c,e}\cot\theta_e - Z_{c,o}\cot\theta_o} & \frac{j}{2}\frac{Z_{c,e}^2 + Z_{c,o}^2 - 2Z_{c,e}Z_{c,o}(\cot\theta_e\cot\theta_o + \csc\theta_e\csc\theta_o)}{Z_{c,e}\csc\theta_e - Z_{c,o}\csc\theta_o} \\ \frac{2j}{Z_{c,e}\csc\theta_e - Z_{c,o}\csc\theta_o} & \frac{Z_{c,e}\cot\theta_e + Z_{c,o}\cot\theta_o}{Z_{c,e}\cot\theta_e - Z_{c,o}\cot\theta_o} \end{bmatrix}.$$

The removal of the ground conductor corresponds to very large even characteristic impedance $Z_{c,e}$ compared to the odd impedance $Z_{c,o}$. Assumed small electrical lengths (θ_e and θ_o), the ABCD matrix reduces to,

$$\begin{bmatrix} A & B \\ C & D \end{bmatrix} \cong \begin{bmatrix} 1 & j\omega L + \frac{1}{j\omega C} \\ 0 & 1 \end{bmatrix},$$

where $\omega L = Z_{c,e}\theta_e/2$, and $\frac{1}{\omega C} = \frac{Z_{c,o}}{\theta_o}$. This corresponds to a series LC resonant circuit as expected [19], where the inductance L is determined by the even mode parameters, and the capacitance C is determined by the odd mode parameters.

The magnitude and phase of S_{11} of the OSRR equivalent circuit model [19] are shown in Fig. 10. On the same figure, the magnitude and phase of S_{11} of the coupled line model are also shown. The width and separation are the same as of the OSRR, the length is the average between the inner and outer radii after subtracting the microstrip gap ($l = 11.66$ mm). To model the etching of the ground, a suspended stripline configuration is considered. The air layer above and below the substrate, in the suspended stripline defined in Ansoft designer circuit simulator student version, is 5 mm height. These parameters correspond to: $Z_{c,e} = 485\,\Omega$, $Z_{c,o} = 110\,\Omega$, $\epsilon_{e,e} = 1.27$, and $\epsilon_{e,o} = 1.7$. Excellent agreement can be observed between the two models at the lower resonance frequency (3.24 GHz). Moreover, the coupled line model is capable to predict the second resonance of the OSRR, which is due to its distributed nature [18].

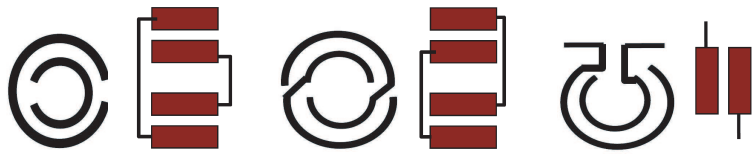

(a) Edge-coupled (b) Non bianisotropic (c) Open -SRR

Figure 9. Different SRR configurations and their coupled line equivalent circuit models.

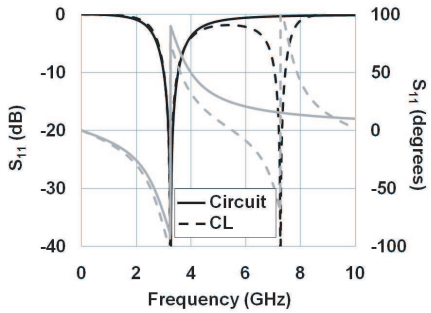

Figure 10. SRR simulations: Solid line is the L, C as described in [19], dashed line is the coupled line model as described here, black is the magnitude, and grey is the phase.

This configuration of OSRR has been selected in this comparison because it is directly coupled to the host transmission line. For other SRR shapes, the coupling scheme between the SRR and host line is included in the equivalent inductor and capacitor model. The coupling schemes reduce the reliability of the existing geometrical model as was shown in [19].

Complementary CSRR can also be modeled using the coupled lines. In this case, two short-circuited slotlines, i.e., network 6, model the CSRR. The even mode does not exist as well since it is a two-conductor structure. The proposed coupled line models can be extended to model other SRR and CSRR shapes.

Comparing the coupled line CRLH to SRR-cells, the coupled line cells rely on the presence of the two modes to create the CRLH behavior. This generally occurs when the effective length of the coupled lines is comparable to $\lambda/4$ or its multiples. Coupled line CRLHs have geometrical models, yet, the values of the even and odd mode impedances are not always achievable in practice. In SRRs and CSRRs, the effect of the even mode is significantly reduced by removing the third conductor. The LH band can only be created if SRRs and CSRRs (or vias) are combined together. Although, the SRR unit cells have compact size, yet, they need double-layer processing and/or the insertion of large number of vias to create LH bands.

6. CONCLUSION

The conventional 12 2-port coupled line networks were studied from filter and CRLH perspectives. For each network, the dispersion relation and Bloch impedance were calculated, and the filter behavior was determined. The advantages of these unit cells are the simple

realization and the presence of a geometrical circuit model. The presence of the LH bands allows the realization of CRLH structures as was shown in [9]. This paper is an attempt to bridge the gap between filter and CRLH researchers [20].

ACKNOWLEDGMENT

This work was supported by the Science and Technology Development Fund (STDF), Egypt, under contract number 48.

REFERENCES

1. Caloz, C., "Dual composite right/left-handed (D-CRLH) transmission line metamaterial," *IEEE Microwave and Wireless Components Letters*, Vol. 16, No. 11, 585–587, 2006.
2. Eleftheriades, G. V., "A generalized negative-refractive-index transmission-line (NRI-TL) metamaterial for dual-band and quad-band applications," *IEEE Microwave and Wireless Components Letters*, Vol. 17, No. 6, 415–417, 2007.
3. Duran-Sindreu, M., A. Velez, F. Aznar, G. Siso, J. Bonache, and F. Martin, "Applications of open split ring resonators and open complementary split ring resonators to the synthesis of artificial transmission lines and microwave passive components," *IEEE Transactions on Microwave Theory and Techniques*, Vol. 57, No. 12, 3395–3403, 2009.
4. Jones, E. and J. T. BollJahn, "Coupled-strip-transmission-line filters and directional couplers," *IEEE Transactions on Microwave Theory and Techniques*, Vol. 4, No. 2, 75–81, 1956.
5. Zysman, G. and A. Johnson, "Coupled transmission line networks in an inhomogeneous dielectric medium," *IEEE Transactions on Microwave Theory and Techniques*, Vol. 17, No. 10, 753–759, 1969.
6. Nguyen, H. and C. Caloz, "Generalized coupled-mode approach of metamaterial coupled-line couplers: Coupling theory, phenomenological explanation, and experimental demonstration," *IEEE Transactions on Microwave Theory and Techniques*, Vol. 55, No. 5, 1029–1039, 2007.
7. Abdelaziz, A. F., T. M. Abuelfadl, and O. L. Elsayed, "Leaky wave antenna realization by composite right/left-handed transmission line," *Progress In Electromagnetics Research Letters*, Vol. 11, 39-46, 2009.
8. Safwat, A. M. E., "Microstrip coupled line composite right/left-handed unit cell," *IEEE Microwave and Wireless Components Letters*, Vol. 19, No. 7, 434–436, 2009.

9. Fouda, A. E., A. M. Safwat, and H. El-Hennawy, "On the applications of the coupled-line composite right/left-handed unit cell," *IEEE Transactions on Microwave Theory and Techniques*, Vol. 58, No. 6, 1584–1591, 2010.
10. Abdelaziz, A., T. Abuelfadl, and O. Elsayed, "Realization of composite right/left-handed transmission line using broadside coupled coplanar waveguides," *2009 IEEE Antennas and Propagation Society International Symposium*, 1–4, Charleston, SC, 2009.
11. Collin, R. E., *Foundations for Microwave Engineering*, 2nd edition, Wiley-IEEE Press, Dec. 2000.
12. Velez, A., J. Bonache, and F. Martin, "Varactor-loaded complementary split ring resonators (VLCSRR) and their application to tunable metamaterial transmission lines," *IEEE Microwave and Wireless Components Letters*, Vol. 18, No. 1, 28–30, 2008.
13. Safwat, A. M. E., "High impedance wire composite right/lefthanded transmission lines," *Microwave and Optical Technology Letters*, Vol. 52, No. 6, 1390–1393, 2010.
14. Abdelaziz, A. F., T. M. Abuelfadl, and O. L. Elsayed, "Realization of composite right/left-handed transmission line using coupled lines," *Progress In Electromagnetics Research*, Vol. 92, 299–315, 2009.
15. HFSS, High Frequency Structures Simulator, Ansoft Corporation, Pittsburgh, PA, 2008.
16. Pozar, D. M., *Microwave Engineering*, 3rd edition, John Wiley & Sons Inc, Sep. 2004.
17. Pendry, J., A. Holden, D. Robbins, and W. Stewart, "Magnetism from conductors and enhanced nonlinear phenomena," *IEEE Transactions on Microwave Theory and Techniques*, Vol. 47, No. 11, 2075–2084, 1999.
18. Marques, R., F. Martin, and M. Sorolla, *Metamaterials with Negative Parameter: Theory, Design, and Microwave Applications*, Wiley-Interscience, 2008.
19. Martel, J., R. Marques, F. Falcone, J. Baena, F. Medina, F. Martin, and M. Sorolla, "A new LC series element for compact bandpass filter design," *IEEE Microwave and Wireless Components Letters*, Vol. 14, No. 5, 210–212, 2004.
20. "Metamaterials: A rich opportunity for discovery or an overhyped gravy train?" *IEEE MTT-S Int. Microw. Symp.*, Boston, MS, Jun. 2009.